Generation of 13.9-mJ Terahertz Radiation from Lithium Niobate Materials

Xiaojun Wu, Deyin Kong, Sibo Hao, Yushan Zeng, Xieqiu Yu, Baolong Zhang, Mingcong Dai, Shaojie Liu, Jiaqi Wang, Zejun Ren, Sai Chen, Jianhua Sang, Kang Wang, Dongdong Zhang, Zhongkai Liu, Jiayan Gui, Xiaojun Yang, Yi Xu, Yuxin Leng, Yutong Li, Liwei Song*, Ye Tian*, and Ruxin Li*

Xiaojun Wu, Deyin Kong, Sibo Hao, Yushan Zeng contributed equally to this work.

X. Wu, D. Kong, S. Hao, M. Dai, S. Liu, J. Wang, Z. Ren, S. Chen

School of Electronic and Information Engineering, and School of Cyber Science and Technology, Beihang University, Beijing, 100191, China

E-mail: xiaojunwu@buaa.edu.cn

X. Wu, D. Kong

Zhangjiang Laboratory, 100 Haike Road, Shanghai, 201210, China

Y. Zeng, X. Yu, J. Sang, K. Wang, D. Zhang, J. Gui, X. Yang, Y. Xu, Y. Leng, L. Song*, Y. Tian*, and R. Li

State Key Laboratory of High Field Laser Physics and CAS Center for Excellence in Ultra-intense Laser Science, Shanghai Institute of Optics and Fine Mechanics, Chinese Academy of Sciences, Shanghai, 201800, China

E-mail: slw@siom.ac.cn; tianye@siom.ac.cn

This article has been accepted for publication and undergone full peer review but has not been through the copyediting, typesetting, pagination and proofreading process, which may lead to differences between this version and the Version of Record. Please cite this article as doi: 10.1002/adma.202208947.

Z. Liu

School of Physical Science and Technology, ShanghaiTech University, Shanghai 201210,

China; ShanghaiTech Laboratory for Topological Physics, Shanghai 201210, China

B. Zhang, Y. Li

Beijing National Laboratory for Condensed Matter Physics, Institute of Physics, Chinese Academy of Sciences, Beijing, 100190, China

X. Wu

Wuhan National Laboratory for Optoelectronics, Huazhong University of Science and Technology, Wuhan 430074, China.

Keywords: terahertz generation, ultrafast phenomena, nonlinear optics, tilted pulse-front technique

Abstract: Extremely strong-field terahertz (THz) radiation in free space has compelling applications in nonequilibrium condensed matter state regulation, all-optical THz electron acceleration and manipulation, THz biological effects, etc. However, these practical applications are constrained by the absence of high-intensity, high-efficiency, high-beam-quality, and stable solid-state THz light sources. Here, the generation of single-cycle 13.9-mJ extreme THz pulses from cryogenically cooled lithium niobate crystals and a 1.2% energy conversion efficiency from 800 nm to THz were demonstrated experimentally using the tilted pulse-front technique driven by a home-built 30-fs, 1.2-Joule Ti:sapphire laser amplifier. The focused peak electric field strength was estimated to be 7.5 MV/cm. We also produced a record of 1.1-mJ THz single-pulse energy at a 450 mJ pump at room temperature and observed that the self-phase modulation of the optical pump could induce THz saturation behavior from the crystals in the substantially nonlinear pump regime. This study lays the foundation for the generation of sub-Joule THz radiation from lithium niobate crystals and will inspire more innovations in extreme THz science and applications.

1. Introduction

Terahertz (THz) radiation with exceptionally strong fields, ultrafast temporal resolution, and specific photon energies is consistent with the characteristic resonance energy level in condensed matter. THz technology has already permitted a variety of applications in electron acceleration and manipulation,[1–5] nonequilibrium matter state studies,[6–12] and high-field biological effects[13–16]. Over the past half-century, the efficient scaling up of THz energy and strong THz fields in free space has sparked considerable research interest. The ubiquity of femtosecond laser-driven intense THz sources has made them one of the most essential next-generation extreme THz radiation facilities. Many millijoule-level THz light sources, which provide unparalleled excitement for extreme THz science and applications, have been demonstrated.[17–22] In addition, these THz devices have exceptional applications in condensed-matter physics and other areas of science. However, the lack of extreme THz light sources with comprehensive characteristics, such as high power, high energy, high efficiency, high beam quality, and high stability, limits the applicability of extremely nonlinear THz research, even with ultrafast laser technology.

In contrast to plasma-based THz sources, lithium niobate material-based strong-field THz sources can be more efficient in producing a higher-quality beam, and their stabilities are synchronized with the pump laser beam, leading to a more user-friendly facility.[22] Lithium niobate materials have a high second-order effective nonlinear susceptibility (~360 pm/V).[23] After doping, large crystals with a high laser-damage threshold can be manufactured. The first THz pulse from a lithium niobate wafer dates back to 1971.[24] The tilted pulse-front technique garnered considerable interest in 2002.[25] The progress of strong-field THz sources for lithium niobate during the last half-century is summarized in **Figure 1**.[22,26–31] It initially increased rapidly from a few microjoules to tens of microjoules. Following the experimental demonstration of 0.4 mJ single pulse energy,[31] advancements had been stymied for several years until the recent achievement of 1.4 mJ from stacked lithium niobate crystals at low temperature driven by a 30-fs Ti:sapphire laser amplifier operating at 214 mJ pump energy.[22] With the rapid advancement of ultrafast laser technology, terawatt-level high-power laser systems operating at a wavelength of 800 nm have emerged[32,33] or

were constructed.[34] These large laser facilities can continuously provide strong pump intensity to generate stronger THz radiation and even inspire researchers to envision the generation of Joule-level THz pulse in free space. Both types of Ti:sapphire laser systems employed in most ultrafast laboratories and those commercially available can produce ultrabroadband spectra with ultrashort pulse durations (≤30 fs). They cause THz energy saturation and decrease the 800 nm-to-THz conversion efficiency when the pump intensity is increased further.[35–37] However, these massive and costly high-energy laser systems are not primarily designed for THz applications. Consequently, ultrashort pulse durations result in intrinsically less efficient THz generation via optical rectification when the tilted pulse-front technique is employed.[38] All these limitations inhibit the realization of higher THz generation from lithium niobate crystals and the development of further extreme THz applications.

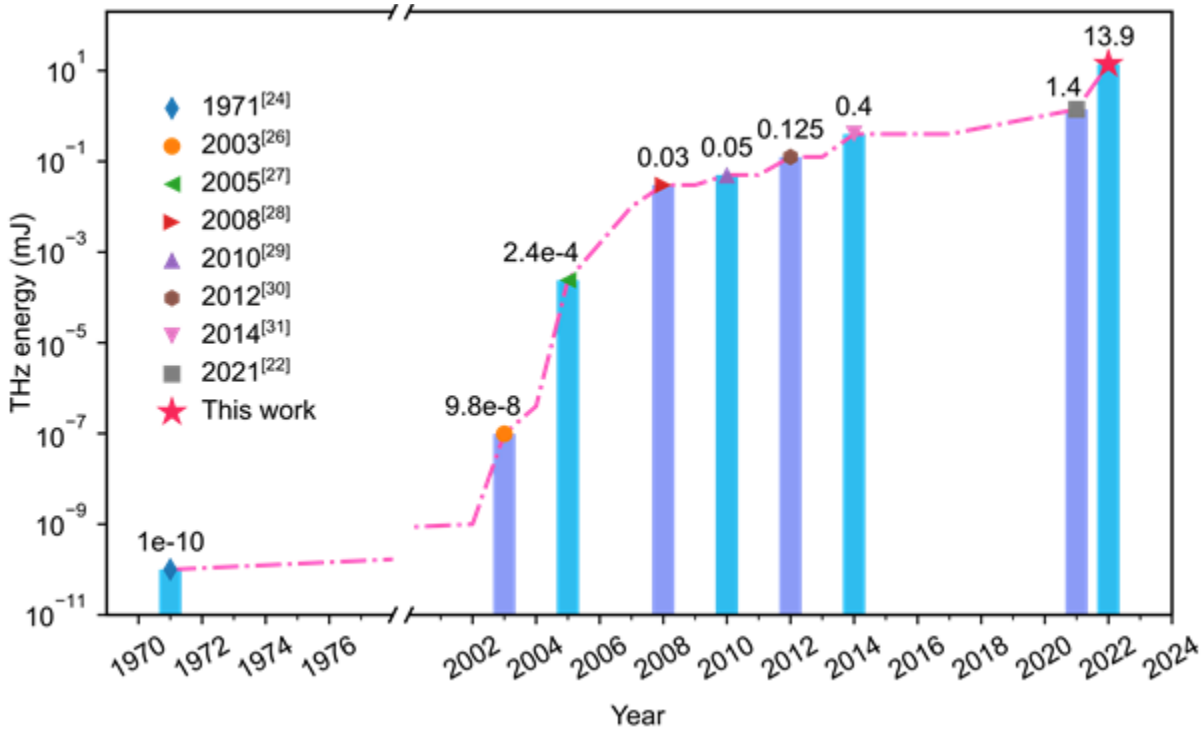

Figure 1 THz output energy milestones obtained from lithium niobate materials via tilted pulse-front technique. All demonstrations are provided with the extracted experimentally realized single-pulse THz energy and reported years.

In this study, we reveal the origin of the ultrashort femtosecond-laser-driven THz efficiency saturation, propose a collaborative compensation linearization mechanism, and experimentally demonstrate an order of magnitude scaling up for the single-cycle THz energy (single pulse energy of 13.9 mJ) from lithium niobate crystals under the excitation of 1.2-J Ti:sapphire femtosecond laser pulses via a tilted pulse-front technique. At room temperature, we obtained a pumping-energy-dependent nonlinear efficiency behavior with almost 1.1-mJ THz output at a pump energy of ~450 mJ (pump fluence of ~40 mJ/cm^2) and efficiency of ~0.4% at a pump energy of ~150 mJ (pump fluence of ~15 mJ/cm^2). When the crystal was cryogenically cooled, the efficiency was further increased to 1.2%, and the THz energy was increased to 13.9 mJ. Self-phase modulation (SPM) was confirmed to be the dominant factor for efficiency saturation in our case through the blue shift in the residual spectra and a simplified one-dimensional plus the frequency axis (1D+1) model.[23] These findings might pave the way for the possibility of strong THz sources, inspiring researchers to envision extreme THz science and applications.

2. System Configuration

The experimental configuration based on the tilted pulse-front technique is illustrated in **Figure 2**a. A home-built Ti:sapphire laser amplifier with 800-nm central wavelength, 30-fs pulse duration, and 1-Hz repetition rate was employed to pump the lithium niobate crystals for high-energy THz generation at room (or low) temperature. The maximum peak power of this laser can reach up to 200 TW. To avoid damaging the optical components, we used a maximum single pulse energy of 1.2 J. To improve the generation efficiency, the spectrum was modulated by a Dazzler. For such ultrashort and high peak power laser pulses, we may need to chirp them to a longer pulse duration by shrinking the distance between grating pairs. The chirped pulses were then reflected into a vacuum chamber and propagated into the THz generation setup through a 10-mm thick antireflection-coated fused silica window. Before the generation of THz pulses, the pump laser spectrum and its beam profile were characterized and well-defined. Figure 2b depicts the pump spectrum with a central wavelength of 800 nm and ~21-nm spectral bandwidth (full width at half

maximum, FWHM). It has a beam profile with a diameter of ~80 mm (FWHM), as shown in Figure 2c, taken using silver-chlorobromide black-and-white photographic paper. For pulse duration measurements, a small fraction of the beam rim was sampled after leaving the compressor, and was then guided through a 5-mm thick fused-silica window to an autocorrelator outside the compressor chamber. Thus, by considering the different window thicknesses and the accumulated second-order group velocity dispersions that the 800 nm pump beam went through, the pulse widths were respectively ~186 fs (for obtaining maximum THz energy) and ~34 fs (at room temperatures) before entering the THz generation setup, whereas they were broadened to ~388 fs (for obtaining maximum THz energy) and ~222 fs (at room temperatures) before entering the lithium niobate crystal with Dewar incidence window mounted. Without Dewar incidence window, the pulse widths before entering the lithium niobate crystal were ~361 fs and ~195 fs, respectively. Detailed calculation processes are described in S8 in Supporting Information. Besides, due to the grating, the pulse duration at the entrance of the crystals is not constant in space. The above calculations should only be used as simple estimations.

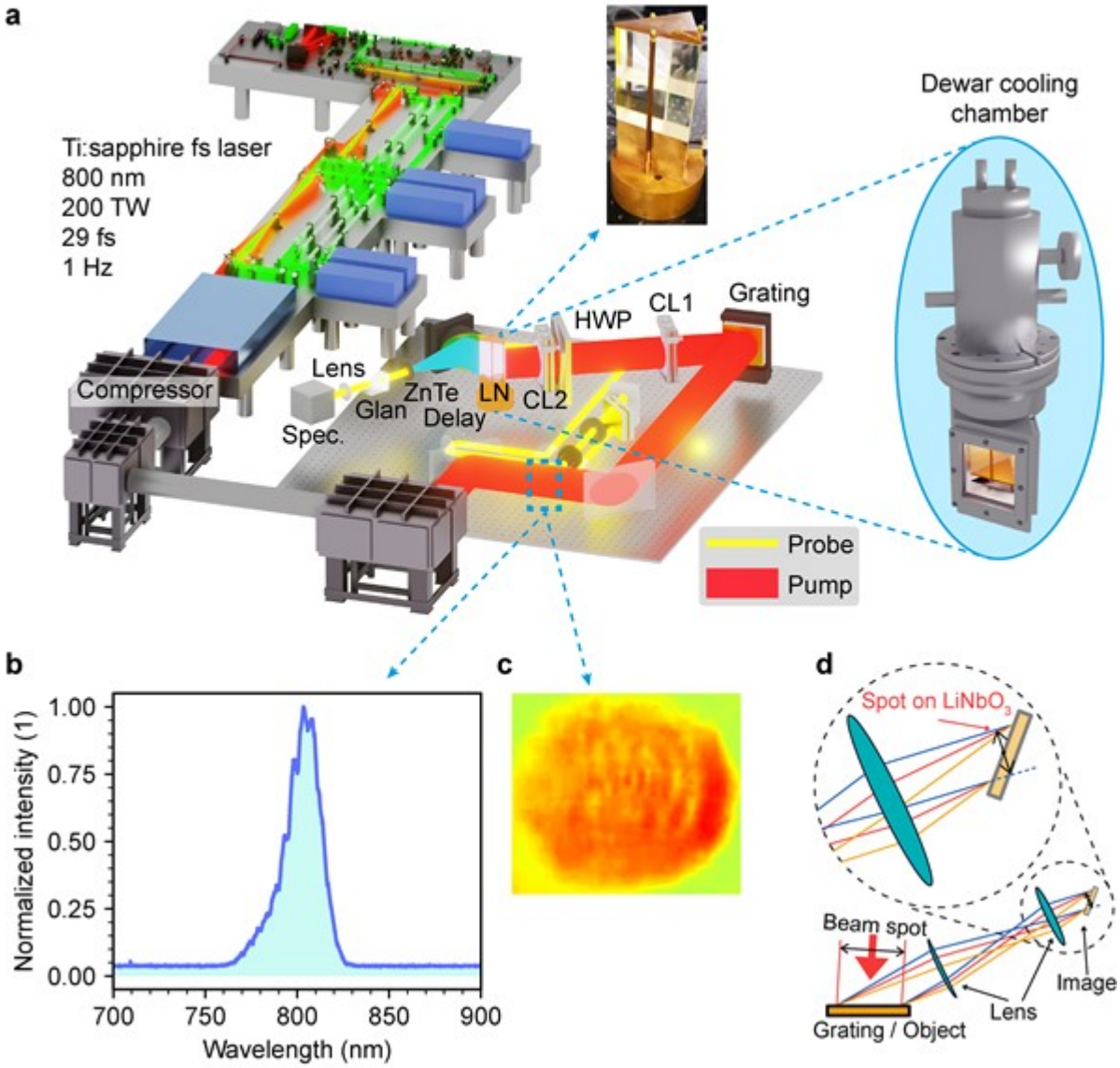

Figure 2 Experiment setup for high energy THz generation. a, Schematic of the pump laser system, which delivers 800-nm central wavelength with 30-fs transform-limited pulse duration at 1-Hz repetition rate with maximum pulse energy of 6 J. The laser spectrum can be adjusted via an acousto-optic programmable dispersive filter for highly efficient THz generation, while the gratings in the compressor are used for chirping the pump pulses. The chirped pulses go through a vacuum chamber and then illuminate onto the grating for the tilted pulse-front technique. The diffracted pump pulses go through two cylindrical lenses (CL1 and CL2) and one half-wave plate (HWP), and

stimulate two vertically stacked congruent lithium niobite crystals. The THz radiation properties are also characterized when the two crystals are cryogenically cooled by liquid nitrogen**. b,** Typical pump spectrum measured before entering the tilted pulse-front setup, and **c,** its typical beam profile acquired by a silver-chlorobromide black-and-white photographic paper. **d,** Geometric optical path diagram for estimating the pump spot size on the crystals.

For the THz generation implementation, the pump laser pulses were guided by two reflection mirrors and illuminated onto a grating with 1200 lines/mm at an incidence angle of 3.4°. The minus one-order diffraction light with >95% diffraction efficiency was passed through two cylindrical lenses (size:105 mm × 105 mm; focus lengths: ~200 mm and ~100 mm) and imaged into two stacked z-cut congruent lithium niobate crystals doped with 6% mol MgO. Each prism has a horizontal plane dimension with a triangle shape of 68.1 mm×68.1 mm×64 mm for each side, while the height of each prism is 40 mm. As shown in Figure 2d, the demagnification factor was 2, and this imaging system guaranteed the phase-matching condition. For the room-temperature experiments, two lithium niobate crystals were tightly stacked, as shown in Figure 2a. They were cryogenically cooled to low temperatures in a Dewar chamber using liquid nitrogen. The radiated THz pulses were collected and focused by a four-inch off-axis parabolic mirror with a focal length of four inches. The THz energy was detected using calibrated pyroelectric detectors (Gentec SDX-1152), and its beam profile was captured using a commercial THz camera (Ophir, Pyrocam IV). To avoid saturating the detectors and the camera, a handmade THz attenuator made of black card paper was inserted before them, and their energy transmittance factor was calibrated (refer to S1 in Supporting Information). To characterize the radiated THz temporal waveform, we built a single-shot spectrum code detection system,[39] which mainly includes a delay line, pulse stretcher with two transmission gratings, Glan prism, and spectrometer. The probing beam was intercepted from the pump beam, and the THz temporal waveform was extracted by comparing the probing spectrum variations with and without THz pulses. The equation $E_{THz} = \frac{U_0}{TR}$ was used to acquire the THz energies, where U_0 is the oscilloscope voltage in volts, T is the total transmission coefficients (considering all the attenuation between the crystal output surface and the THz detector), and R is the response of the THz detector. Two detectors (Detector 1 and Detector 2) were used in our experiments, and their responses were 23.4 V/mJ and 12.2 V/mJ, respectively. More details are shown in the Supporting Information.

3. Room-temperature high-energy THz generation

To determine whether this laser system can produce powerful THz radiation, we investigated the room-temperature THz emission characteristics of lithium niobate crystals. To the best of our knowledge, lithium niobate crystals have not been exposed to several hundred millijoules of high-energy ultrashort laser pulses under these conditions.[40] Consequently, the material can be rapidly pushed into the nonlinear region, resulting in a variety of nonlinear phenomena within the crystals.[41] When the pump power is increased, high-order nonlinear effects may reduce the THz generation efficiency; thus, the system parameters must be optimized at different pump energies. During the optimization of the system, we first attempted to adjust the system and acquire the maximum THz energy at a fixed pump energy of ~81 mJ, defined as the adjusting energy. The pump energy-related THz energy curve was recorded when the system was optimized to its maximum output THz energy. We then adjusted this system at higher pump energies, specified the new adjusting energy, and measured the THz energy curves. **Figure 3**a shows a schematic of the SPM nonlinear effects inside the crystals in the strongly nonlinear pump region. In this region, as summarized in Figure 3b, the THz energies no longer show a linear upward trend but saturate with an increase in pump energy. Interestingly, there is an inflection point in the dependence between the THz energy and pump energy near 150 mJ. To a certain extent, this pump energy is determined by the adjusting energy. However, when the adjusting pump energy is higher than 150 mJ (in our case, 206 and 320 mJ), this inflection point is limited to below 200 mJ. Before the inflection point, the THz energy curve was steep and became flat when the pump fluence passed the inflection point. Consequently, a maximum THz energy of $\frac{U_0}{TR} = \frac{6.86\text{V}}{0.27\times 23.4\text{V/mJ}} \approx 1.1\ \text{mJ}$ is achieved from room-temperature lithium niobate crystals under the excitation of 450-mJ pump pulses. The saturation phenomenon of the THz output energy indicates a decrease in efficiency, which is explicitly depicted in Figure 3c. Under different adjusting pump energies, the efficiency curves initially rise and then decline. Although a higher adjusting energy delivers better efficiency, the maximum room-temperature efficiency decreases from ~0.4% to ~0.3% after exceeding 206 mJ (Figure 3d). Ultimately, the maximum 800 nm-to-THz energy conversion efficiency at room temperature is

~0.4%, which is less than that reported recently by replacing the grating with an echelon to tilt the pulse front.[38]

Such a saturation phenomenon is unusual compared to our previous THz generation implementations, which utilized ultrashort-pulse laser-pumped lithium niobate crystals without vertically focusing the laser spot beam. [42–44] However, this behavior was observed when a tightly focused method was employed.[41] As shown in Figure 3a, we hypothesize that other competitive nonlinear phenomena, such as the SPM effect, occur in the crystals owing to the high-intensity pump, degrading the pump spectrum and lowering the THz radiation efficiency. As shown in Figure 3e, this hypothesis can be tested further by tracking the residual pump spectrum with broadening and blue shifts. At a low pump fluence, the influence of the SPM is negligible, with slightly broader residual spectra. The higher the pump fluence, the broader the residual spectrum, the more the blue shift, and the lower the 800 nm-to-THz conversion efficiency.

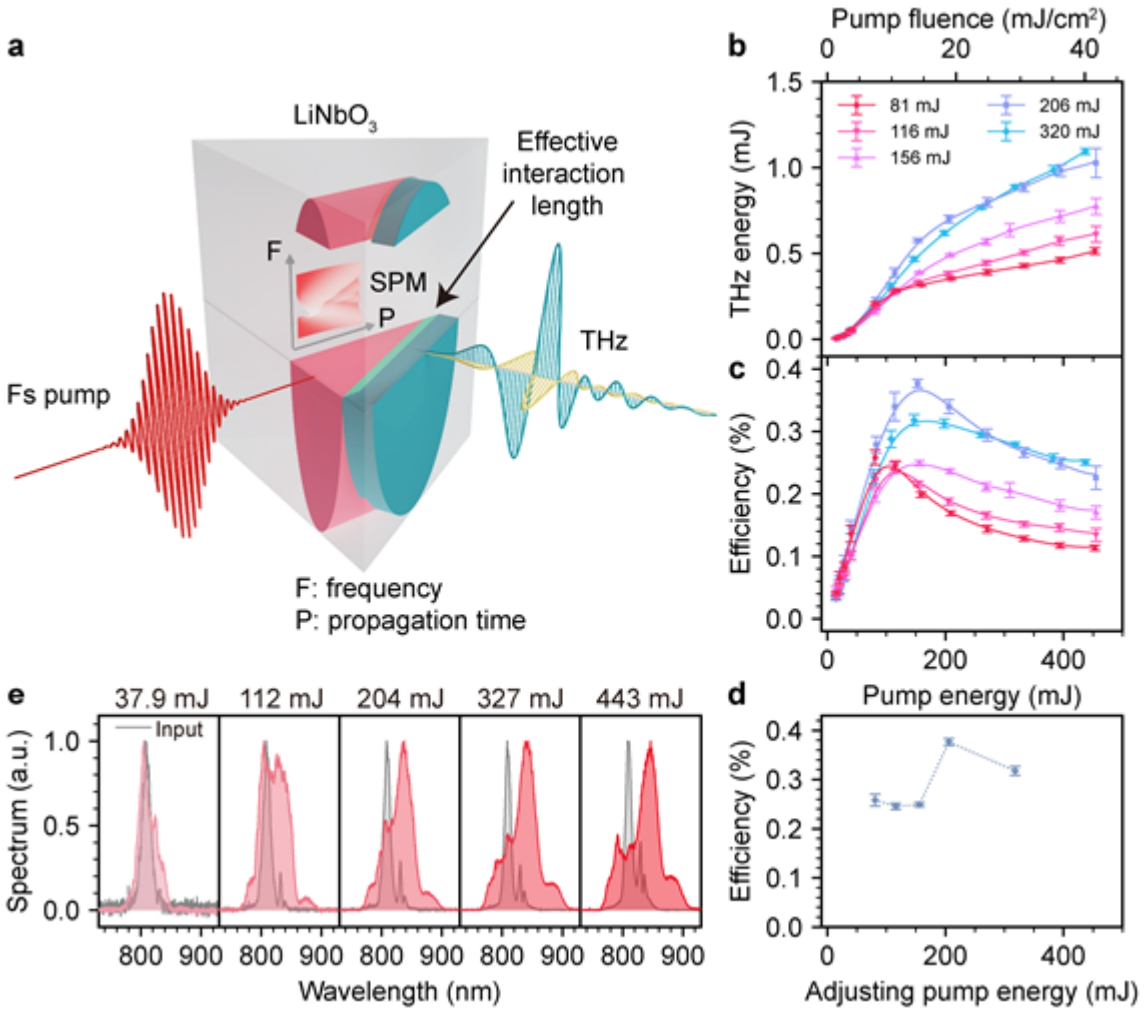

Figure 3 THz radiation from lithium niobate crystals at room temperature. a, Schematic of THz wave generation inside the lithium niobate crystals under strongly nonlinear pump regimes. A typical SPM broadening of the laser is shown, which may cause phase mismatch in the pump spectrum and make it unsuitable for THz generation, causing THz energy saturation and efficiency reduction. **b,** Extracted THz energy as a function of the pump energy (pump fluence) at different adjusting energy with different optimized optical paths, and **c,** corresponding 800 nm-to-THz energy conversion efficiency for different adjusting energies. The transmittance coefficients of 16-layer black card papers for attenuation are 27.6% for adjusting energy from 81 mJ to 206 mJ and 26.8% for 320 mJ. **d,** Maximum 800 nm-to-THz efficiency dependent on the adjusting pump energy for strongly nonlinear pump regimes. **e,** Residual pump spectra with respect to the initial spectrum distribution under different pump energies. The laser spectral broadening may be caused by a combination of SPM and cascading effects. (All measured by Detector 1)

4. Efficiency boosting at low temperatures and the generation of 13.9-mJ THz radiation

We then implemented another cryogenic cooling experiment on the crystals to further corroborate that SPM is the dominant mechanism for efficiency reduction and to obtain a higher THz energy. SPM is a third-order nonlinear effect that occurs in the strong pump region.[41] Lithium niobate crystals exhibit strong lattice absorption in THz waves.[45] Cooling the crystal can significantly reduce linear absorption, thereby enhancing efficiency. Nevertheless, cooling cannot eradicate SPM because it is insensitive to the crystal temperature. At low temperatures, THz efficiency loss and saturation behaviors still occur, validating the SPM effect as the major mechanism responsible for THz energy saturation. As expected, the 800 nm-to-THz efficiency was enhanced to ~0.6% when the crystals were cooled down to ~80 K at an adjusting energy of 320 mJ, as shown in **Figure 4**, and the efficiency saturation pump energy was approximately 100 mJ. These results further validate SPM as the mechanism for efficiency saturation and serve as a reminder that cooling successfully increases efficiency, particularly in the highly nonlinear pump area where SPM is effective.

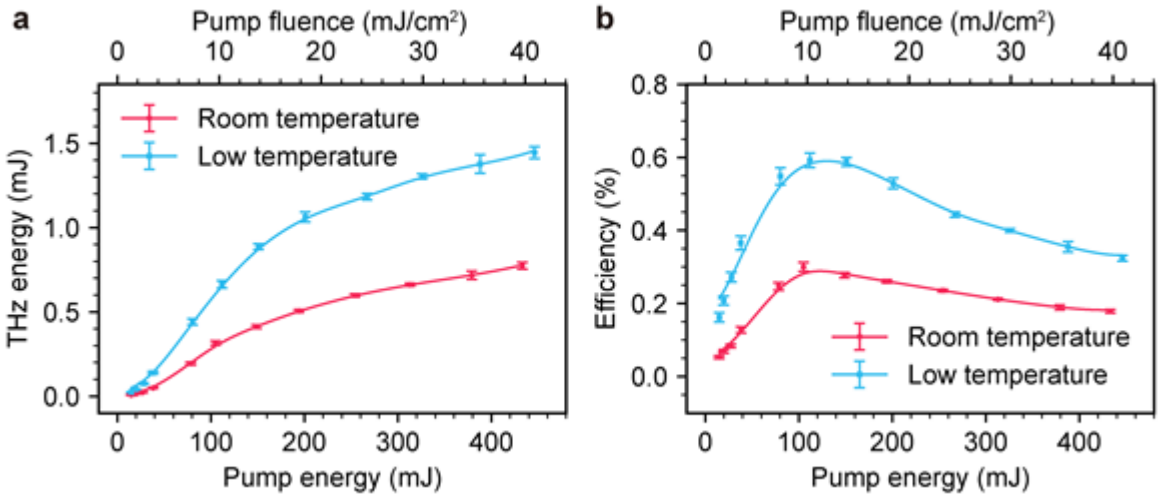

Figure 4 Scaling up the THz efficiency at a low temperature under strongly nonlinear pump regimes. a, THz energy curves and **b,** efficiencies varied with the pump energy recorded at room

(red) and low (blue) temperatures (~ 80 K). Cooling the crystal can increase the THz generation efficiency, but the THz energy saturation still exists at the pump energy (~100 mJ). The transmittance is 25.2% in low temperatures lower than 26.2% at room temperature as the vapor permeates the TPX window of the vacuum chamber. The transmittance of the output TPX window of the vacuum chamber is estimated to be 90%.[46] The pump pulse width was ~222 fs before entering the lithium niobate crystal. (All measured by Detector 1)

The aforementioned THz output energy results were limited by increasing the pump energy or reducing the crystal temperature under ultrashort femtosecond laser pumping. According to the optical-to-THz energy conversion efficiency,[47]

$$\eta_{THz} = \left(\frac{2d_{eff}^2}{\varepsilon_0 n_{opt}^2 n_{THz} c^3}\right) \Omega_{THz}^2 \cdot I \cdot \left[L^2 \, exp\left(\frac{-\alpha L}{2}\right) \cdot \frac{\sinh^2\left(\frac{\alpha L}{4}\right)}{\left(\frac{\alpha L}{4}\right)^2}\right] \#(1)$$

where η_{THz} is the generated THz efficiency, d_{eff} is the effective nonlinear coefficient, ε_0 is the vacuum permittivity, n_{opt} is the optical refractive index of lithium niobate at 800 nm, while n_{THz} is the THz frequency band, c is the speed of light in vacuum, Ω_{THz} is the THz angular frequency, I is the pump intensity, L is the effective interaction length, and α represents the THz absorption coefficient. To obtain a higher radiation efficiency and stronger THz energy, we need to optimize the pump intensity, crystal absorption, and effective interaction length. Among them, the effective interaction length is, in turn, significantly affected by the pump intensity and pump spectral distribution owing to the nonlinear distortion effect.[48] Therefore, the strongly correlated influences of various parameters lead to difficulties in generating high-energy THz pulses with high efficiency. To overcome other competitive nonlinear effects during the THz generation process, we implemented a collaborative compensation method by further chirping the pump pulse, carefully optimizing the pump spectrum, and fine-adjusting the elliptical pump spot shape at low temperatures. Using this optimization method, we successfully overcome the adverse effects of SPM and realize a quasi-linear increase in the THz energy output. **Figure 5**a shows the extracted THz energy as a function of the pump fluence/energy, which manifests as a linear increase. A maximum THz energy of $\frac{U_0}{TR} = \frac{12.2\text{V}}{(0.08\times0.9)\times12.2\text{V/mJ}} \approx 13.9\ \text{mJ}$ was obtained under excitation of ~1.2 J (126 mJ/cm^2). Compared with

our reported 1.4 mJ lithium niobate crystals, this result raises the THz energy by an order of magnitude, which is the first solid-state THz source with >10-mJ single pulse energy. In addition to achieving highly single-pulse energy, we enhanced the THz efficiency with a maximum value of 1.2% under excitation of 1 J (refer to Figure 5b). Upon further increasing the pump energy to 1.2 J, the efficiency exhibits a slight saturation behavior without dramatically decreasing the tendency. This implies that the radiated THz energy can be further increased as long as some damage not occurs in the optical components.

To further calculate the focused THz electric field strength and diagnose its peak frequency, we built a single-shot spectrum coding setup and measured the radiated THz temporal waveform (refer to S2 in the Supporting Information). Figure 5c depicts the restored THz transient signal with a single-cycle temporal waveform and the pulse duration (FWHM) of ~3.8 ps. Figure 5d plots the corresponding spectrum, and its peak frequency is approximately 0.2 THz. This low center frequency may be caused by the long THz propagation distance in large crystals. Figure 5e shows the focused THz beam profile, its major and minor axis were 2.68 mm and 2.36 mm, respectively. The focused THz field strength can be estimated to be ~7.5 MV/cm (refer to S3 in the Supporting Information).

THz energy stability is also crucial for practical applications. Figure 5f shows the stability measurement results before we increased the pump energy to 1.2 J and optimized the system to achieve the highest efficiency. During the 2000 s test period, the THz energy fluctuated slightly with a standard deviation of 0.1 mJ corresponding to a fluctuation of 2.5%. Generally, the stability of a lithium niobate crystal-based THz light source is mainly determined by the pump laser. Our home-built 200 TW laser system is quite stable, which ensures subsequent extreme THz application experiments.

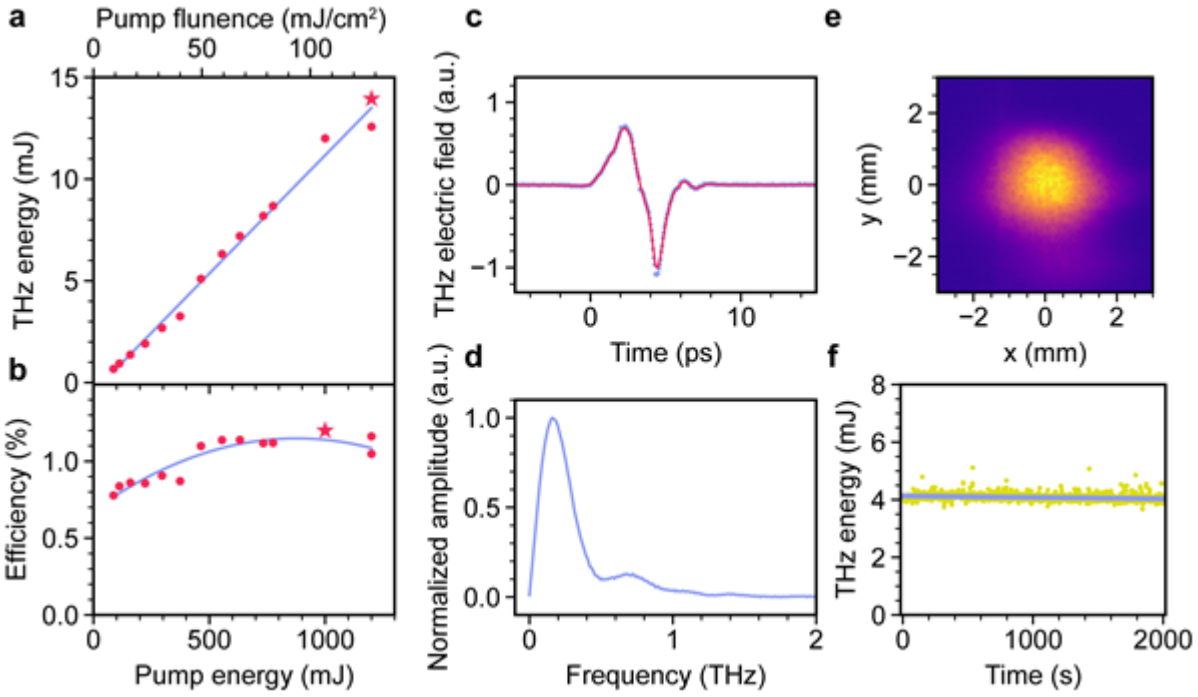

Figure 5 13.9-mJ THz radiation from cryogenically cooled lithium niobate crystals at 1.2-J pump. a, Detected THz energy with a blue linear-fitting curve and **b**, its corresponding efficiency with a blue quadratic-polynomial-fitting curve as a function of the pump energy. The transmittance coefficients of the attenuator made of 27-layer black card papers are about 8%. The maximum THz energy of 13.9 mJ is obtained under the pump energy of 1.2 J, while the highest efficiency of 1.2% under 1.0-J pump energy. **c,** Measured THz temporal signal data with its smoothed waveform, and **d,** its corresponding Fourier-transformed spectrum. The waveform is smoothed to reduce system error caused by the low resolution of laser spectroscopy and signal retrieval. **e,** Focused THz beam profile manifests an elliptical shape with a 2.68-mm major axis (FWHM) and 2.36-mm minor axis (FWHM). **f,** Stability measurement lasts 2000 s under the pump energy of ~700 mJ, with a blue linear-fitting curve. For stability measurement, only 10 black card papers are pasted for attenuation, and the transmittance is 24.5%. (All measured by Detector 2)

Although we could obtain an even higher THz energy output via the collaborative compensation optimization approach, optics damage impedes further scaling up of the pump energy. The first easy-to-destroy optics may be the vacuum chamber window, which may also cause damage to the grating in the THz generation setup. Therefore, in this case, the pump energy is limited to 1.2 J.

However, the experimental results obtained here imply opportunities and challenges for Joule-level extreme THz generation from lithium niobate crystals.

5. Numerical calculation of the efficiency saturation caused by SPM

To demonstrate the influence of SPM on the THz generation efficiency, we used a simplified 1D+1 model that considers[23] (i) material dispersion for the pump laser and THz wave (at room temperature), (ii) angular dispersion of the pump laser, (iii) absorption at THz frequency, (iv) SPM, and (v) different propagation directions of the pump laser and the generated THz wave. This model neglects the geometry of the crystal, cascaded down-conversion, and up-conversion of the optical frequency and focuses on the influence of SPM. This model can be calculated by solving the modified nonlinear Schrödinger equations using the split-step Fourier method.[49] More details about this deduction can be found in Section S6 of the Supporting Information.

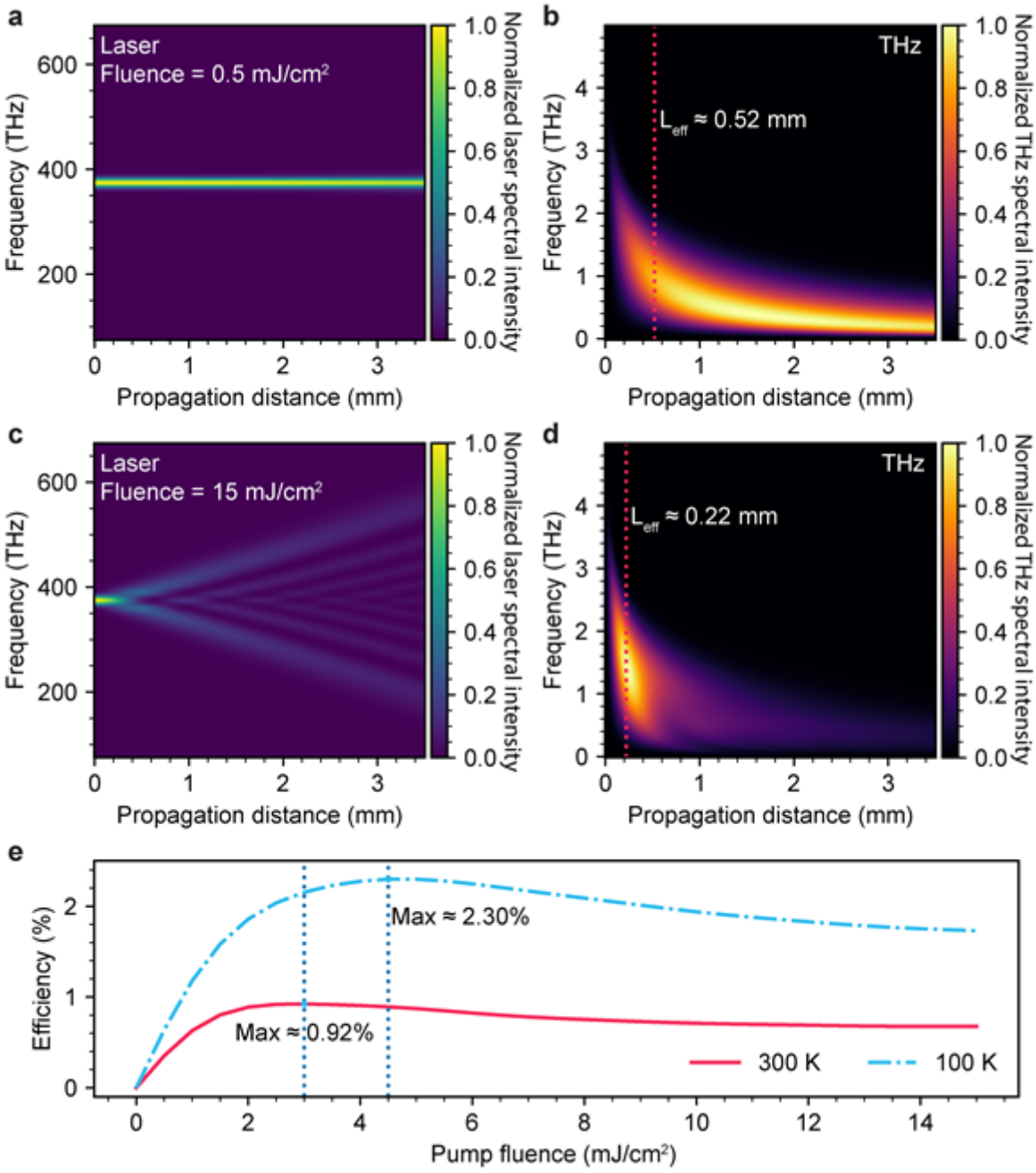

Figure 6 Numerical analysis of the influence of SPM on the THz generation. a and **c**, Evolution of normalized laser spectra with the fluence of 0.5 mJ/cm^2 and 15 mJ/cm^2 during the propagation at 300 K, respectively. **b** and **d,** Corresponding evolution of normalized THz spectra. All the spectra in the crystal are calculated using $|Electric\ field|^2$ and normalized by respective maximum values. **e,**

800 nm-to-THz efficiency changes with the pump fluence calculated at the propagation distance of 3.5 mm.

For pump lasers with a fluence of ~0.5 mJ/cm^2, as shown in **Figure 6**a, the spectrum broadening caused by SPM during the propagation is not evident. However, if the fluence increases to ~15 mJ/cm^2, the influence of the SPM is significant, where the width of the laser spectra changes from ~25 THz at the start position to ~470 THz after propagating for ~3.5 mm. This prominent SPM phenomenon is mainly due to the short pulse width of ~30 fs, which is in agreement with experiments conducted at room temperatures. Figure 6b and 6d show the corresponding THz spectra. The effective interaction length can be defined as the distance measured in the THz propagation direction from the beginning of propagation to where the 800 nm-to-THz efficiency is maximized. As shown in Figures 6b and d, the effective interaction length L_{eff} for the pump fluence of ~15 mJ/cm^2 (L_{eff} =0.22 mm) is shorter than that for the pump fluence of ~0.5 mJ/cm^2 (L_{eff} =0.52 mm). As illustrated in Figure 6d, the amplitude of the THz signal is reduced faster than that in Figure 6b. There are three possible explanations for this phenomenon. First, the broadened laser spectrum and the shifted phase caused by SPM may lead to destructive interference between the generated THz fields at different propagation distances. A high pump fluence may exacerbate spectrum deterioration (phase mismatch or unsuitable energy distribution of the pump spectrum) and decay of the THz signal. Second, if the laser spectrum is broadened, a large amount of laser energy is carried to high and low frequencies. The material properties will change if the frequency is far from the center frequency, where the phase-match condition may not be satisfied, and the THz generation efficiency decreases. Finally, when the pump fluence increases, as shown in Figures 6b and d, the frequency of the THz spectrum peak value at the distance L_{eff} at a low fluence (~1 THz) moves to a higher frequency (~1.5 THz) owing to the SPM. The absorption of the THz wave is stronger at high frequencies than at low frequencies; therefore, the total absorption increases with a high fluence, which causes a faster decay of the THz wave in Figure 6d than in Figure 6b. Figure 6e indicates that the calculated 800 nm-to-THz efficiency changes with pump fluence. These saturation efficiencies (~0.92% and ~2.30% at the fluence of ~3.0 mJ/cm^2 and ~4.5 mJ/cm^2 at 300 K and 100 K, respectively) demonstrate the influence of the SPM, although they do not accord with the measured

~15 mJ/cm^2. This difference from the experimental results may be caused by the cascaded frequency-conversion effect neglected by our model. The actual laser spectrum, along with the laser chirp, may also affect the SPM, and thus affect the saturation of the 800 nm-to-THz efficiency. Further investigations are required to obtain a more accurate numerical analysis.

5. Conclusion

We investigated the generation of intense THz radiation from lithium niobate crystals using Ti:sapphire femtosecond laser excitation at ambient and low temperatures. By optimizing the device, modulating the spectrum, and chirping the pump laser, a maximum generation efficiency of 1.2% was obtained, and the retrieved THz single-pulse energy of 13.9 mJ at low temperature is a new record, representing an order of magnitude improvement over what we had previously accomplished. Moreover, high THz radiation can be steady when coordinated with the driving laser system. Saturation of the 800 nm-to-THz efficiency was observed during the experiment, which might be attributed to SPM, as evidenced by the experimental results and numerical analysis. Compared to other high-energy THz sources, lithium niobate crystals are more appropriate for creating high-energy THz radiation because of their strong nonlinear coefficients, large manufacturing size, high damage threshold, and pump wavelength compatibility. We expect that the 13.9 mJ solid-state THz generator demonstrated in this study will enable essential nonlinear studies and a multitude of extreme applications hitherto unattainable in this valuable frequency regime.

6. Experimental Section/Methods

Laser system: THz generation is driven by a self-constructed Ti:sapphire laser system that provides 6-J, 30-fs laser pulses at a 1-Hz repetition rate. The laser system comprised a Ti:sapphire oscillator, Öffner stretcher, regenerative amplifier, power amplifier, and a vacuum compressor.[50] An acousto-optic programmable dispersive filter (AOPDF) was employed after the oscillator to optimize the laser spectrum for THz generation, and the vacuum compressor was tuned to maximize the laser-THz conversion efficiency.

Single-shot THz characterization: Single-shot measurement based on spectral coding was employed to characterize the radiated THz temporal waveform, as illustrated in Figure. 2a. For this measurement, a one-inch reflection mirror was intercepted at the edge of the pump beam to obtain a small partial energy as a probing beam. It was further stretched using a stretcher comprising a pair of gratings. Subsequently, a delay line was used to synchronize both the probing beam and radiated THz signal. The probing beam was focused along with the THz onto a 1-mm thick electro-optic crystal ZnTe by an off-axis parabolic mirror with a focal length of four inches. A Glan prism was used to purify the polarization of the probe beam. Consequently, the probing beam spectrum was collected and analyzed using a high-precision fiber spectrometer (Ocean Optics USB4000). By retrieving the spectral signal, the THz temporal transient is extracted by decoding the spectrum recorded by the spectrometer.[22]

Tilted pulse front theory: For lithium niobate crystals, the refractive index at an optical wavelength of 800 nm is smaller than that at the THz frequency band. The normal incidence of femtosecond laser pulses can cause a serious phase mismatch between the THz wave and pump laser, which causes destructive interference of the THz radiation generated by the cascading effect and decreases the optical-to-THz conversion efficiency. The tilted pulse-front technique aims to solve this phase-matching problem. By tilting the wavefront of the pump laser, the phase velocity of the THz wave could be matched with the group velocity of the laser wavefront. This method also provides a way to easily improve the energy and size of the laser beam spot.[25]

SPM induced 800 nm-to-THz efficiency saturation and numerical analysis: SPM is a nonlinear optical effect that adds a phase change to the laser pulse and broadens the laser spectrum, caused by the intensity-dependent refractive index interacting with the ultrafast pulse;[51] the higher the pump fluence, the shorter the distance the laser can propagate without substantial spectral degradation and the shorter the effective interaction length for THz generation. This effect decreases the THz

efficiency and causes efficiency saturation. We used a 1D+1 model along with the split-step Fourier method[49] to analyze the influence of the SPM on the 800 nm-to-THz efficiencies. Detailed calculation processes are provided in the Supporting Information.

Supporting Information

Supporting Information is available either from the Wiley Online Library or author.

Acknowledgements

Supported by the National Key R&D Program of China (2022YFA1604402), the National Natural Science Foundation of China (11827807, 92250307, 11127901), Technology Innovation Action Plan of the Science and Technology Commission of Shanghai Municipality with project number 20JC1416000, the Open Project Program of Wuhan National Laboratory for Optoelectronics NO.2022WNLOKF006.

Author contribution: X. Wu, D. Kong, S. Hao, and Y. Zeng contributed equally to this study.

X.W., L.S., and Y.T. conceived and coordinated the strong-field THz generation and application project. D.K., S.H., B.Z., J. S., and K. W. designed the experimental setup and performed the experiments. Y. Z., X. Y., and D. Z. maintained the laser propagation system and contributed helpful discussions to the experiments. D.K. performed simulations for THz generation, and M.D. performed the simulation for the electron gun. J. G, X. Y., Y. X., Y. L., and R. L. built and operated the 200-TW laser system. X.W., D.K., S.H., M.D., J.Q.W., and L.S. wrote and revised the manuscript.

Received: ((will be filled in by the editorial staff))
Revised: ((will be filled in by the editorial staff))
Published online: ((will be filled in by the editorial staff))

References

[1] C. Kealhofer, W. Schneider, D. Ehberger, A. Ryabov, F. Krausz, P. Baum, *Science* **2016**, *352*, 429.

[2] D. Zhang, A. Fallahi, M. Hemmer, X. Wu, M. Fakhari, Y. Hua, H. Cankaya, A.-L. Calendron, L. E. Zapata, N. H. Matlis, F. X. Kärtner, *Nat. Photonics* **2018**, *12*, 336.

[3] M. T. Hibberd, A. L. Healy, D. S. Lake, V. Georgiadis, E. J. H. Smith, O. J. Finlay, T. H. Pacey, J. K. Jones, Y. Saveliev, D. A. Walsh, E. W. Snedden, R. B. Appleby, G. Burt, D. M. Graham, S. P. Jamison, *Nat. Photonics* **2020**, *14*, 755.

[4] H. Tang, L. Zhao, P. Zhu, X. Zou, J. Qi, Y. Cheng, J. Qiu, X. Hu, W. Song, D. Xiang, J. Zhang, *Phys. Rev. Lett.* **2021**, *127*, 74801.

[5] H. Xu, L. Yan, Y. Du, W. Huang, Q. Tian, R. Li, Y. Liang, S. Gu, J. Shi, C. Tang, *Nat. Photonics* **2021**, *15*, 426.

[6] T. Dong, S. Li, M. Manjappa, P. Yang, J. Zhou, D. Kong, B. Quan, X. Chen, C. Ouyang, F. Dai, J. Han, C. Ouyang, X. Zhang, J. Li, Y. Li, J. Miao, Y. Li, L. Wang, R. Singh, W. Zhang, X. Wu, *Adv. Funct. Mater.* **2021**, *31*, 2100463.

[7] E. A. Mashkovich, K. A. Grishunin, R. M. Dubrovin, A. K. Zvezdin, R. V. Pisarev, A. V. Kimel, *Science* **2021**, *374*, 1608.

[8] C. Bao, P. Tang, D. Sun, S. Zhou, *Nat Rev Phys* **2022**, *4*, 33.

[9] Q. Li, V. A. Stoica, M. Paściak, Y. Zhu, Y. Yuan, T. Yang, M. R. McCarter, S. Das, A. K. Yadav, S. Park, C. Dai, H. J. Lee, Y. Ahn, S. D. Marks, S. Yu, C. Kadlec, T. Sato, M. C. Hoffmann, M. Chollet, M. E. Kozina, S. Nelson, D. Zhu, D. A. Walko, A. M. Lindenberg, P. G. Evans, L.-Q. Chen, R. Ramesh, L. W. Martin, V. Gopalan, J. W. Freeland, J. Hlinka, H. Wen, *Nature* **2021**, *592*, 376.

[10] M. B. Heindl, N. Kirkwood, T. Lauster, J. A. Lang, M. Retsch, P. Mulvaney, G. Herink, *Light: Sci. Appl.* **2022**, *11*, 5.

[11] S. Schlauderer, C. Lange, S. Baierl, T. Ebnet, C. P. Schmid, D. C. Valovcin, A. K. Zvezdin, A. V. Kimel, R. V. Mikhaylovskiy, R. Huber, *Nature* **2019**, *569*, 383.

[12] C. Meineke, M. Prager, J. Hayes, Q. Wen, L. Z. Kastner, D. Schuh, K. Fritsch, O. Pronin, M. Stein, F. Schäfer, S. Chatterjee, M. Kira, R. Huber, D. Bougeard, *Light: Sci. Appl.* **2022**, *11*, 151.

[13] Y. Li, C. Chang, Z. Zhu, L. Sun, C. Fan, *J. Am. Chem. Soc.* **2021**, *143*, 4311.

[14] T. Tachizaki, R. Sakaguchi, S. Terada, K.-I. Kamei, H. Hirori, *Opt. Lett.* **2020**, *45*, 6078.

[15] A. A. Greschner, X. Ropagnol, M. Kort, N. Zuberi, J. Perreault, L. Razzari, T. Ozaki, M. A. Gauthier, *J. Am. Chem. Soc.* **2019**, *141*, 3456.

[16] P. Zalden, L. Song, X. Wu, H. Huang, F. Ahr, O. D. Mücke, J. Reichert, M. Thorwart, P. K. Mishra, R. Welsch, R. Santra, F. X. Kärtner, C. Bressler, *Nat. Commun.* **2018**, *9*, 2142.

[17] G.-Q. Liao, H. Liu, G. G. Scott, Y.-H. Zhang, B.-J. Zhu, Z. Zhang, Y.-T. Li, C. Armstrong, E. Zemaityte, P. Bradford, D. R. Rusby, D. Neely, P. G. Huggard, P. McKenna, C. M. Brenner, N. C. Woolsey, W.-M. Wang, Z.-M. Sheng, J. Zhang, *Phys. Rev. X* **2020**, *10*.

[18] A. D. Koulouklidis, C. Gollner, V. Shumakova, V. Y. Fedorov, A. Pugžlys, A. Baltuška, S. Tzortzakis, *Nat. Commun.* **2020**, *11*, 292.

[19] Y. Tian, J. Liu, Y. Bai, S. Zhou, H. Sun, W. Liu, J. Zhao, R. Li, Z. Xu, *Nat. Photonics* **2017**, *11*, 242.

[20] S. W. Jolly, N. H. Matlis, F. Ahr, V. Leroux, T. Eichner, A.-L. Calendron, H. Ishizuki, T. Taira, F. X. Kärtner, A. R. Maier, *Nat. Commun.* **2019**, *10*, 2591.

[21] J. A. Fülöp, S. Tzortzakis, T. Kampfrath, *Adv. Optical Mater.* **2020**, *8*, 1900681.

[22] B. Zhang, Z. Ma, J. Ma, X. Wu, C. Ouyang, D. Kong, T. Hong, X. Wang, P. Yang, L. Chen, Y. Li, J. Zhang, *Laser Photonics Rev.* **2021**, *15*, 2000295.

[23] K. Ravi, W. R. Huang, S. Carbajo, X. Wu, F. Kärtner, *Opt. Express* **2014**, *22*, 20239.

[24] K. H. Yang, P. L. Richards, Y. R. Shen, *Appl. Phys. Lett.* **1971**, *19*, 320.

[25] J. Hebling, G. Almasi, I. Kozma, J. Kuhl, *Opt. Express* **2002**, *10*, 1161.

[26] A. G. Stepanov, J. Hebling, J. Kuhl, *Appl. Phys. Lett.* **2003**, *83*, 3000.

[27] A. Stepanov, J. Kuhl, I. Kozma, E. Riedle, G. Almási, J. Hebling, *Opt. Express* **2005**, *13*, 5762.

[28] A. G. Stepanov, L. Bonacina, S. V. Chekalin, J.-P. Wolf, *Opt. Lett.* **2008**, *33*, 2497.

[29] A. G. Stepanov, S. Henin, Y. Petit, L. Bonacina, J. Kasparian, J.-P. Wolf, *Appl. Phys. B* **2010**, *101*, 11.

[30] J. A. Fülöp, L. Pálfalvi, S. Klingebiel, G. Almási, F. Krausz, S. Karsch, J. Hebling, *Opt. Lett.* **2012**, *37*, 557.

[31] J. A. Fülöp, Z. Ollmann, C. Lombosi, C. Skrobol, S. Klingebiel, L. Pálfalvi, F. Krausz, S. Karsch, J. Hebling, *Opt. Express* **2014**, *22*, 20155.

[32] C. N. Danson, C. Haefner, J. Bromage, T. Butcher, J.-C. F. Chanteloup, E. A. Chowdhury, A. Galvanauskas, L. A. Gizzi, J. Hein, D. I. Hillier, N. W. Hopps, Y. Kato, E. A. Khazanov, R. Kodama, G. Korn, R. Li, Y. Li, J. Limpert, J. Ma, C. H. Nam, D. Neely, D. Papadopoulos, R. R. Penman, L. Qian, J. J. Rocca, A. A. Shaykin, C. W. Siders, C. Spindloe, S. Szatmári, R. M. G. M. Trines, J. Zhu, P. Zhu, J. D. Zuegel, *High Pow Laser Sci Eng* **2019**, *7*, 255.

[33] Z. Gan, L. Yu, C. Wang, Y. Liu, Y. Xu, W. Li, S. Li, L. Yu, X. Wang, X. Liu, J. Chen, Y. Peng, L. Xu, B. Yao, X. Zhang, L. Chen, Y. Tang, X. Wang, D. Yin, X. Liang, Y. Leng, R. Li, Z. Xu, in *Progress in Ultrafast Intense Laser Science XVI*, Vol. 141 (Eds.: K. Yamanouchi, K. Midorikawa, L. Roso), Springer International Publishing. Cham **2021**, p. 199.

[34] Ford Burkhart, *High-power lasers to work with lab's X-ray laser to boost understanding of matter*, https://optics.org/news/12/10/31.

[35] D. Jang, C. Kang, S. K. Lee, J. H. Sung, C.-S. Kee, S. W. Kang, K.-Y. Kim, *Opt. Lett.* **2019**, *44*, 5634.

[36] D. Jang, J. H. Sung, S. K. Lee, C. Kang, K.-Y. Kim, *Opt. Lett.* **2020**, *45*, 3617.

[37] L. Wang, G. Tóth, J. Hebling, F. Kärtner, *Laser Photonics Rev.* **2020**, *14*, 2000021.

[38] L. Guiramand, J. E. Nkeck, X. Ropagnol, T. Ozaki, F. Blanchard, *Photon. Res.* **2022**, *10*, 340.

[39] Z. Jiang, X. C. Zhang, *Opt. Lett.* **1998**, *23*, 1114.

[40] X.-J. Wu, J.-L. Ma, B.-L. Zhang, S.-S. Chai, Z.-J. Fang, C.-Y. Xia, D.-Y. Kong, J.-G. Wang, H. Liu, C.-Q. Zhu, X. Wang, C.-J. Ruan, Y.-T. Li, *Opt. Express* **2018**, *26*, 7107.

[41] S. B. Bodrov, A. A. Murzanev, Y. A. Sergeev, Y. A. Malkov, A. N. Stepanov, *Appl. Phys. Lett.* **2013**, *103*, 251103.

[42] X. Wu, S. Carbajo, K. Ravi, F. Ahr, G. Cirmi, Y. Zhou, O. D. Mücke, F. X. Kärtner, *Opt. Lett.* **2014**, *39*, 5403.

[43] X. Wu, A.-L. Calendron, K. Ravi, C. Zhou, M. Hemmer, F. Reichert, D. Zhang, H. Cankaya, L. E. Zapata, N. H. Matlis, F. X. Kärtner, *Opt. Express* **2016**, *24*, 21059.

[44] B. Zhang, S. Li, S. Chai, X. Wu, J. Ma, L. Chen, Y. Li, *Photon. Res.* **2018**, *6*, 959.

[45] X. Wu, C. Zhou, W. R. Huang, F. Ahr, F. X. Kärtner, *Opt. Express* **2015**, *23*, 29729.

[46] V. E. Rogalin, I. A. Kaplunov, G. I. Kropotov, *Opt. Spectrosc.* **2018**, *125*, 1053.

[47] J. Hebling, A. G. Stepanov, G. Almsi, B. Bartal, J. Kuhl, *Appl. Phys. B* **2004**, *78*, 593.

[48] C. Lombosi, G. Polónyi, M. Mechler, Z. Ollmann, J. Hebling, J. A. Fülöp, *New J. Phys.* **2015**, *17*, 83041.

[49] R. Deiterding, R. Glowinski, H. Oliver, S. Poole, *J. Lightwave Technol.* **2013**, *31*, 2008.

[50] F. Wu, Z. Zhang, X. Yang, J. Hu, P. Ji, J. Gui, C. Wang, J. Chen, Y. Peng, X. Liu, Y. Liu, X. Lu, Y. Xu, Y. Leng, R. Li, Z. Xu, *Opt. Laser Technol.* **2020**, *131*, 106453.

[51] R. H. Stolen, C. Lin, *Phys. Rev. A* 1978, *17*, 1448.

The generation of single-cycle 13.9-mJ extreme THz pulses from cryogenically cooled lithium niobate crystals and 1.2% energy conversion efficiency from 800 nm to THz were demonstrated experimentally using the tilted pulse front technique driven by a home-built 30-fs, 1.2-Joule Ti:sapphire laser amplifier. The focused peak electric field strength was estimated to be 7.5 MV/cm.

X. Wu*, D. Kong, S. Hao, Y. Zeng, X. Yu, B. Zhang, M. Dai, S. Liu, J. Wang, Z. Ren, S. Chen, J. Sang, K. Wang, D. Zhang, Z. Liu, J. Gui, X. Yang, Y. Xu, Y. Leng, Y. Li, L. Song*, Y. Tian*, and R. Li

Generation of 13.9-mJ Terahertz Radiation from Lithium Niobate Materials

Toc figure